Seamless Transition between Grid Forming and Grid Following Inverters based on Online Grid Impedance Estimation

Yadala Pavankumar[1*], Xi Luo[1], Efstratios Batzelis[1], Abhinav Singh[1], Georgia Saridaki[2], Panos Kotsampopoulos[2], and Nikos Hatziargyriou[2]

[1]School of Electronics and Computer Science, University of Southamton, Southampton, UK
[2]School of Electrical and Computer Engineering, National Technical University of Athens, Greece
**p.k.yadala@soton.ac.uk*

***Abstract*— The rapid increase in the penetration of inverter-based resources (IBRs) into the distribution network causes the power system to behave as a weak grid and often alters system strength. IBRs operate as either grid-following (GFL) or grid-forming (GFM) inverters, differing in both control stability and inertia support capabilities under varying operating conditions. To maintain system stability across different grid strengths, IBRs need to support smooth switching between GFL and GFM modes. This paper presents an automatic smooth-switching control strategy based on online grid impedance estimation to enhance operational stability. Ordinary Least Squares (OLS) regression is used to estimate grid impedance, and hysteresis switching is applied to prevent continuous switching when grid strength fluctuates near boundary conditions. The effectiveness of the proposed control strategy is verified through case studies under varying grid strengths.**

Keywords—Grid-following inverter, Grid impedance estimation, Grid-forming inverter, Ordinary least squares regression, Smooth switching.

I. INTRODUCTION

The massive increment in the penetration of the inverter-based resources (IBRs) into grid results in rapid change in the stability and characteristics of the entire system. The most common control strategies of the IBRs are either grid-following (GFL) or grid-forming (GFM) mode [1]. The GFL regulates the power injection while acting as a current source inverter and locks into the voltage angle of the grid [2]. On the other hand the GFM generates its own voltage reference signal and independently regulates the frequency and voltage while operating as a voltage source inverter [3]. The GFL inverter does not inherently provide inertia support, but with the integration of additional levels of control, it can offer virtual inertia by adjusting its active power output in response to frequency variations. However, GFL suffers from stability issues under weak grid conditions with low short-circuit ratio (SCR). Conversely, while GFM provides better inertia support, it performs poorly under strong grid conditions due to its behavior as a voltage source that directly regulates the PCC voltage. In such conditions, conflicts between the inverter control and the tightly regulated grid dynamics can cause instability and diminish effective power-sharing capabilities [4], [5]. Given the differing operational characteristics of GFL and GFM, IBRs should have the flexibility to switch their control modes under varying grid conditions to enhance stability and ensure continuous operation.

The literature presents different control strategies for seamless transition from GFL to GFM; most of them are focused on the transition from grid connected to islanded mode [6], [7], [8]. The methods utilize two controllers to provide the reference signals for two modes but at a time only one controller remain active and can switch the mode of operation depending on the requirement. However, these studies ignored the requirement of the operational flexibility of the IBRs connected to the grid. Under varying operational grid conditions, it is necessary to have a mode switching between GFL and GFM to enhance the operational stability. The authors in [9], [10] presented a seamless transition control between GFL and GFM while the converter is still connected to the grid. Smooth switching is achieved by synchronizing the phase angle and current references sent to the current controller, as the inner current controller is common for both GFL and GFM modes. Both GFL and GFM controls run in parallel, ensuring that common signals will always remain synchronized. As the grid strength varies when a change in generation, load, or transmission lines occurs, a valid automatic criterion for mode switching, which is not specified in the above studies, can prevent instability under certain conditions and lead to a more efficient and coordinated grid operation.

The existing literature shows that GFL performs poorly under low SCR, while GFM struggles at higher SCR; therefore, it is beneficial to apply automatic mode switching based on SCR. The challenging part here is to estimate the SCR which involves the estimation of the grid impedance. The literature presents several methods to estimate the grid impedance which are classified as active and passive estimation methods. The active estimation methods [11], [12] inject the perturbation signal into the system and estimate the grid impedance while passive estimation methods [13] use the information inherent in the system. However, these methods are not applied for GFL/GFM mode switching so far.

Therefore, from the existing literature it is clear that there is a need for a control strategy which can automatically switch the mode between GFL and GFM under varying grid strengths. To address this research gap, this paper presents an automatic switching between GFL and GFM based on online grid impedance estimation. Ordinary Least Squares (OLS) regression is used to estimate the SCR, assuming a linear and stationary relationship between voltage and current [14]. OLS is computationally simpler and more accessible compared to complex methods like Kalman filters or machine learning, which require dynamic model of the network. The main contributions of this work are:

- A background synchronisation scheme is proposed which achieve the smooth switching between GFL and GFM modes.
- OLS regression is used to estimate the SCR online.
- Hysteresis switching is applied to avoid the continuous switching at the boundaries of SCR

II. METHODOLOGY

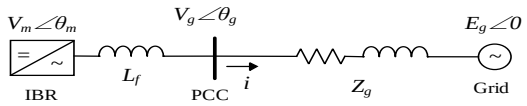

Fig. 1. Grid connected IBR model

A. *System Configuration*

The test system considered in this study is shown in Fig.1. Through a L filter (L_f) the IBR is connected to grid and Z_g represents the grid impedance. The IBR can operate either in GFL mode or GFM mode. In GFL mode, the phase locked loop (PLL) has been used for the grid synchronization and for primary frequency response frequency-droop *P(f)* is applied as shown in Fig.2(a). The current references for the current controller are formulated by translating the power set points into current commands. On the other hand, in GFM mode the reference voltage and frequency are formed by using the standard droop function *f(P)* as shown in Fig.2(b) which drives both the grid synchronization and frequency response.

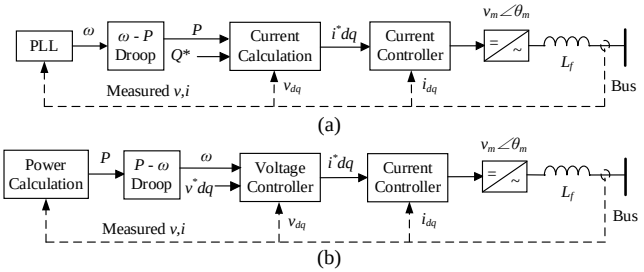

Fig. 2. Control diagrams for IBR in (a) GFL mode and (b) GFM mode.

B. *Analysis of Factors effecting the switching between GFL and GFM*

From the equivalent model of the test system as shown in Fig. 1, the change in Z_g will cause the change in the SCR, which creates the requirement of the mode change of the IBR control. The internal current controller is same for both GFL and GFM control as shown in Fig. 2, therefore the GFL and GFM can generate separate current references which are used as references for the current controller. Similarly, for the grid synchronization the GFL generates the phase angle θ_{gfl} through PLL and GFM generates the θ_{gfm} via droop function. Hence, the mode switching can be done by running both GFL and GFM parallelly and switching the two signals which are (i) current signals before the current controller and (ii) the phase angle (θ) signal.

During the switching process, firstly the phase angle θ may vary. For instance, if the IBR adopted GFM mode, it relies on droop function to generate the phase angle. Meanwhile, the GFL control parameters cannot form a closed loop since there is no feedback. And due to the cumulative effect of the integrator, θ_{gfl} will be different from the current phase angle (θ_{gfm}) of the IBR as shown in Fig. 3(a). Therefore, when the IBR switches from GFM to GFL it causes a sudden change in the θ which results in large fluctuations in the power output. The same applies to the current references. At a time only the active control mode will operate normally, and the other control mode cannot establish a closed loop. Therefore, the current references generated by the inactivated control (GFL) cannot correspond to the actual current references (GFM) as shown in Fig. 3(b) and 3(c), results in sudden change in the current references (I_{dref} and I_{qref}) during switching creates power fluctuations. Secondly, the generation of the switching signal is important under varying grid strengths, failure of generation of accurate switching

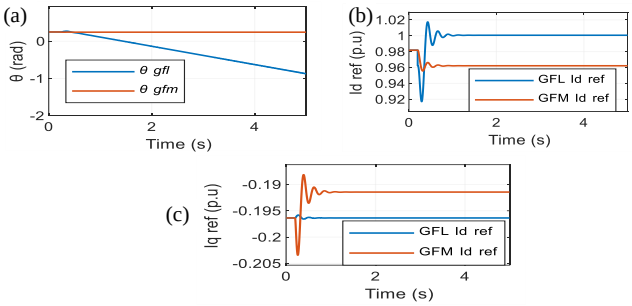

Fig. 3. Without background synchronization (a) phase angle, (b) d-axis current reference and (c) q-axis current reference.

signal may allow the IBR to operate in undesired mode which can deteriorate the operational stability of the system.

C. *Proposed control strategy for automatic switching*

The proposed control strategy consists of two parts. Firstly, to tackle the disturbances caused by the sudden change in phase angle and current references, a smooth switching control strategy is implemented with the help of background controllers and secondly to generate the automatic switching signal an OLS regression-based SCR estimation is used.

i) Smooth switching control strategy: As shown in Fig.5(a), the phase angle smooth switching works as follows: if the IBR operates under GFL mode, all the switches are placed at 1 hence $\theta = \theta_{gfl}$, at the same time in GFM phase angle control block, the background synchronization will be activated (in blue color) which synchronizes the w_{gfm} with w (which is w_{gfl}) therefore at any point of time $w_{gfm} = w = w_{gfl.}$ and $\theta = \theta_{gfl} = \theta_{gfm}$ as shown in Fig. 4(a). When the IBR switched to GFM all the switches will be placed at 0 and since $\theta = \theta_{gfl} = \theta_{gfm}$ there won't be a sudden change in θ.. Similarly, for the current references as illustrated in Fig. 5(b), if IBR operates under GFL mode, all the switches are in 1 which makes I_{dref}=I_{dref_gfl} and I_{qref}=I_{qref_gfl}. The control loop tracks the *P(f)* droop and reactive power droop to obtain the I_{dref_gfl} and I_{qref_gfl} as shown in the equation (1). At the same time in GFM control, the background controller synchronizes the inactive mode current references (I_{dref_gfm} and I_{qref_gfm}) with the active mode current references (I_{dref_gfl} and I_{qref_gfl}) therefore at any point of time $I_{dref\_gfm} = I_{dref\_gfl}$ and $I_{qref\_gfm} = I_{qref\_gfl}$ as shown in Fig. 4(b) and 4(c). As the current references are synchronized there will be no abrupt change during switching. Likewise, the same mechanism works in vice versa when IBR operates in GFM mode as illustrated in Fig. 5.

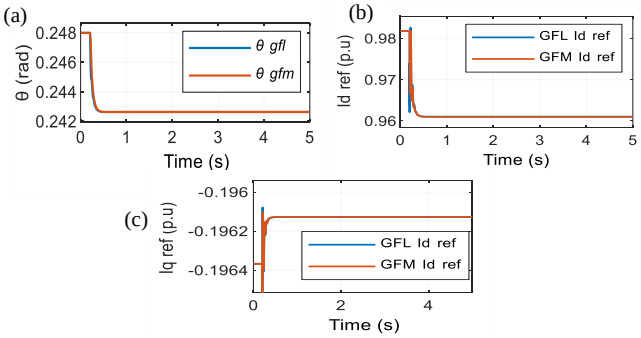

Fig. 4. With background synchronization (a) phase angle, (b) d-axis current reference and (c) q-axis current reference.

Thus, by integrating the smooth switching control strategy for both current references and phase angle, seamless switching is achieved between GFL and GFM.

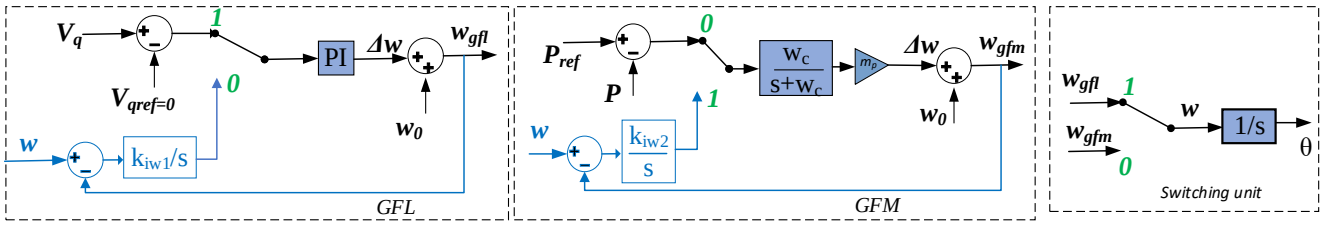

Fig. 5(a). Control block diagram for the phase angle smooth switching.

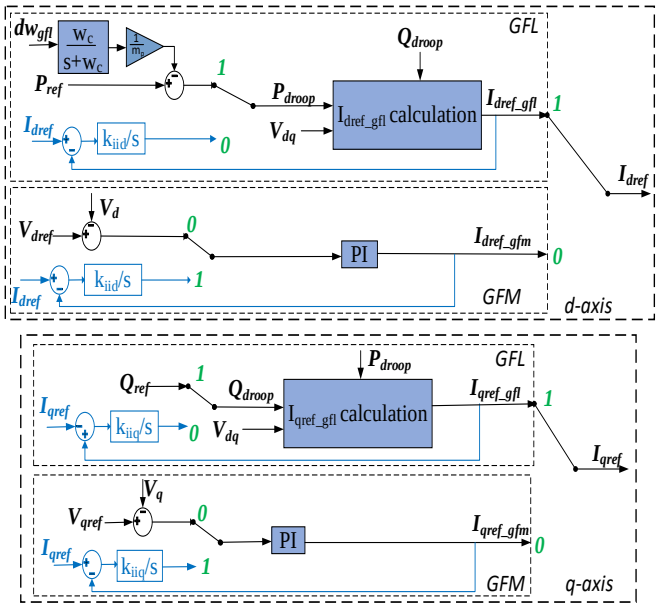

Fig. 5(b). Control block diagram for the d and q axis current references smooth switching.

$$I_{dref\_gfl} = (P_{droop}.V_d + Q_{droop}.V_q)/(V_d^2 + V_q^2)$$
$$I_{qref\_gfl} = (P_{droop}.V_q - Q_{droop}.V_d)/(V_d^2 + V_q^2) \quad (1)$$

ii) SCR estimation and switching signal generation: The switching signal is generated as either 1 (GFL) or 0 (GFM) based on the grid strength i,e. SCR. In the view of operational differences in GFL and GFM, when the SCR is below 3 it is beneficial to operate the IBR in GFM mode, when the SCR is above 6 it should be in GFL mode and if SCR is between 3 and 6 it will follow the previous mode of operation to avoid the unnecessary switching as shown in Fig. 6 because both GFL and GFM can operate efficiently in that phase.

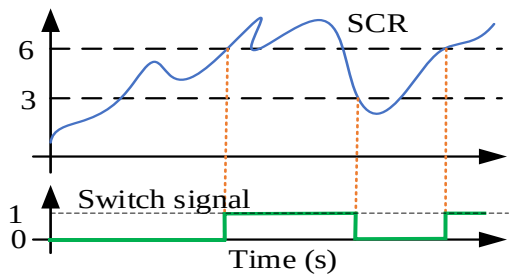

Fig.6. Hysteresis switching mechanism.

For the network considered in Fig. 1, the SCR can be calculated as shown in equation (2).

$$SCR = \frac{P_{sc}}{P_n} = \frac{|E_g|^2}{|Z_g|.P_n} \quad (2)$$

where P_{sc} is the short-circuit power, P_n is the nominal power, E_g and Z_g are the grid voltage and impedance. From equation (2) to estimate the SCR, the grid impedance Z_g needs to be estimated. From Fig. 1, the equation of the measured voltage at the PCC in the phasor domain can be given in equation (3).

$$\bar{V}_g = \bar{i}.\bar{Z}_g + \bar{E}_g \quad (3)$$

where $\bar{V}_g = V_d + jV_q$ and $\bar{i} = i_d + ji_q$. the PCC voltage and current ($\bar{V}_g$ and $\bar{i}$) are measured and sampled within a window period, such that there is approximately a linear relationship between the voltage and current, therefore the estimation of $\bar{Z}_g$ becomes a linear least squares problem with a single solution given symbolically by equation (4)[14].

$$\bar{Z}_g = (\bar{i}^{*T}.\bar{i})^{-1}.\bar{i}^{*T}.\bar{V}_g \quad (4)$$

where $\bar{V}_g$ and $\bar{i}$ are matrices and note that $\bar{i}$ is a matrix with first column as a vector of ones. The PCC voltage and current are sampled at 20ms; the window length for the OLS is considered as 500ms to match with the period of perturbation. A 2% sinusoidal perturbation with 2Hz frequency has been considered in the active power reference. A single frequency sinusoidal perturbation is considered due to its ability to focus on single frequency, less harmonic distortion and minimal system disruption. The mechanism in OLS is designed in such a way that for every 20ms, a new sample goes into the OLS and old sample goes out; hence, the OLS window moves for every 20ms and estimates the grid impedance. The estimated grid impedance will pass through the moving average filter to eliminate the noise and then the SCR will be calculated, depending on the estimated SCR, the hysteresis switching signal is generated as illustrated in Fig. 7. It is note worthy to mention that the window for moving average filter is considered as 1s and the saturation limits are considered for estimated grid impedance to avoid the large fluctuations.

TABLE 1. SYSTEM PARAMETERS

Parameters	**Values**
Base power	10MVA
Frequency of the system (f_o)	50Hz
Active power reference of IBR (P_{ref})	1 p.u
Reactive power reference of IBR (Q_{ref})	0.2 p.u
PLL proportional gain (k_p)	1
Integral gain of PLL (k_i)	500
Droop coefficient (m_p)	2%
Low pass filter cut of frequency (f_c)	20Hz
Current controller proportional gain (k_{pi})	1.25
Current controller integral gain (k_{ii})	10
Voltage control proportional gain(k_{pv})	3
Voltage control integral gain (k_{iv})	100
Gain of phase angle synchronization control (k_{iw1}, k_{iw2})	5000,3000
Gain of d-axis current synchronization control (k_{iid})	100
Gain of q-axis current synchronization control (k_{iiq})	100

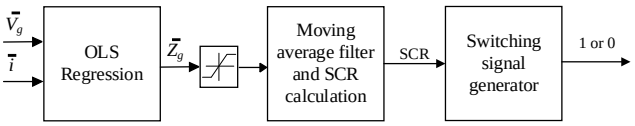

Fig. 7. SCR estimation and switching signal generation.

III. Simulation Results

To validate the proposed control strategy for automatic switching between GFL and GFM, the test system illustrated in Fig. 1 was simulated in MATLAB/SIMULINK. The system parameters considered in this study are given in Table 1 and the resistive part is neglected in grid impedance. Two case studies are considered to evaluate the proposed control strategy, in the first case the gradual change in SCR is considered and in the second case a sudden change in SCR is considered.

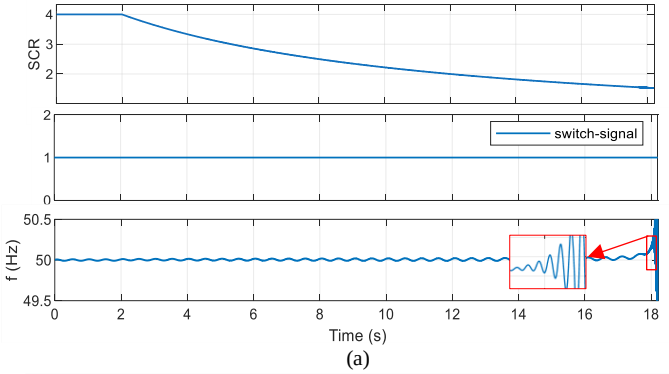

(a)

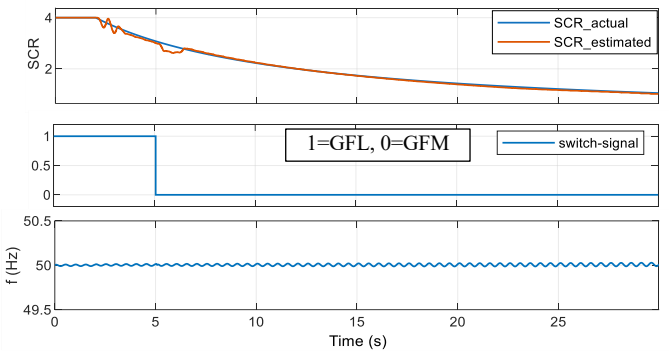

(b)

Fig. 8. System response during gradual decrease in SCR (a) without and (b) with proposed control strategy.

A. *Case 1: Gradual change in SCR:*

Initially it is assumed that the IBR is operating in GFL mode and the SCR started to decrease gradually (theoretically made up) as shown in Fig. 8(a). From Fig. 8(a), as the SCR decreases the GFL struggles and loses the stability around SCR 1.6 without the proposed control strategy. Whereas with proposed control strategy, as shown in Fig. 8(b) the estimated SCR is almost in match with actual SCR as the moving average filter effectively removes the noise and at 5.08s it detects that the SCR dropped below 3 and sends the switching signal to the IBR to change the mode from GFL to GFM and maintains the system operational stability as shown in Fig. 8(b). Moreover, it is assumed that the SCR is increasing gradually, and the IBR is operating as GFM as shown in Fig. 9(a). From Fig.9(a) as the SCR crosses above 8, the GFM failed to maintain the stability without the proposed control strategy. But with the proposed control strategy, the estimated SCR crosses 6 at 14.2s and the mode to GFL and maintains the system stability as shown in Fig. 9(b).

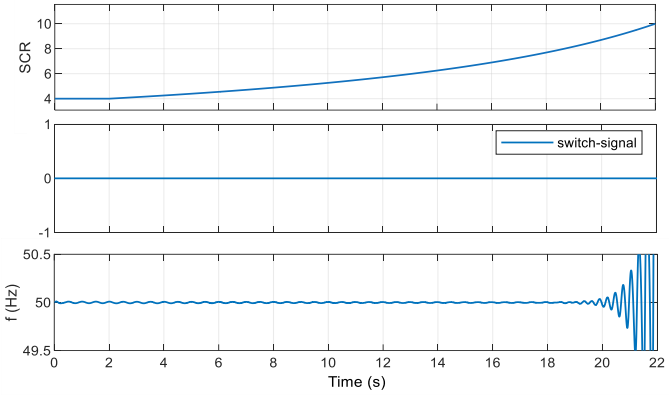

(a)

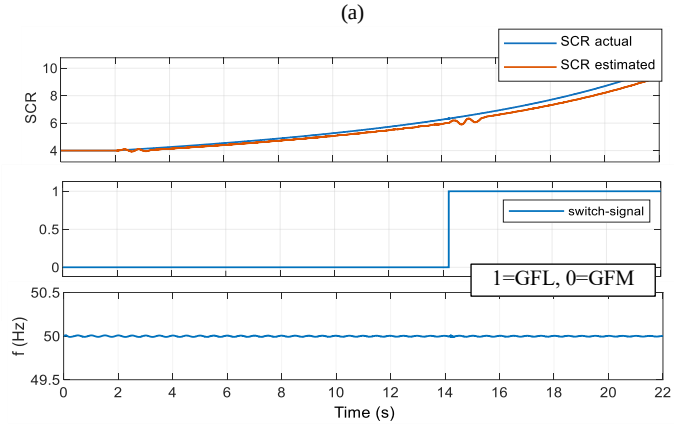

(b)

Fig. 9. System response during gradual increase in SCR (a) without and (b) with proposed control strategy.

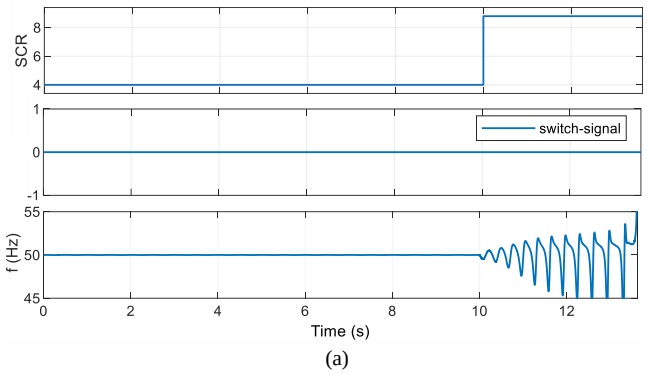

(a)

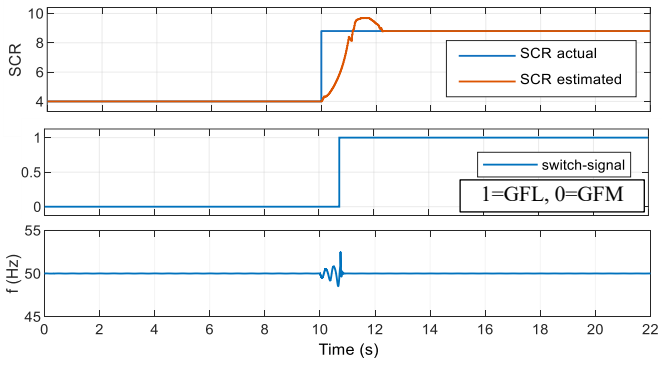

(b)

Fig. 10. System response during sudden increase in SCR (a) without and (b) with proposed control strategy.

B. *Case 2: Sudden change in SCR:*

In this case study the proposed control strategy is tested

under the sudden change in SCR. Firstly, it is assumed that SCR is 4 and IBR operating in GFM mode. At 10s the SCR has increased suddenly to 8.5 (e.g. due to switching in a transmission line), since the IBR is in GFM mode it loses the stability without the mode switching as shown in Fig. 10(a), with the proposed method the change in SCR has been estimated and at 10.52s it detects the SCR has crossed above 6 hence it sends the switching signal to IBR to change the mode to GFL, hence the system becomes stable as shown in Fig. 10(b). And now, it is assumed that the IBR is operating as GFL and the SCR has decreased suddenly from 4 to 1.6, due to very low SCR the GFL based IBR becomes unstable without the mode switching as shown in Fig. 11(a). On the other hand, with the proposed approach, the SCR change is detected at 10.72s and sends the switching signal to the IBR to change its mode to GFM and the system maintains the stability as shown in the Fig. 11(b).

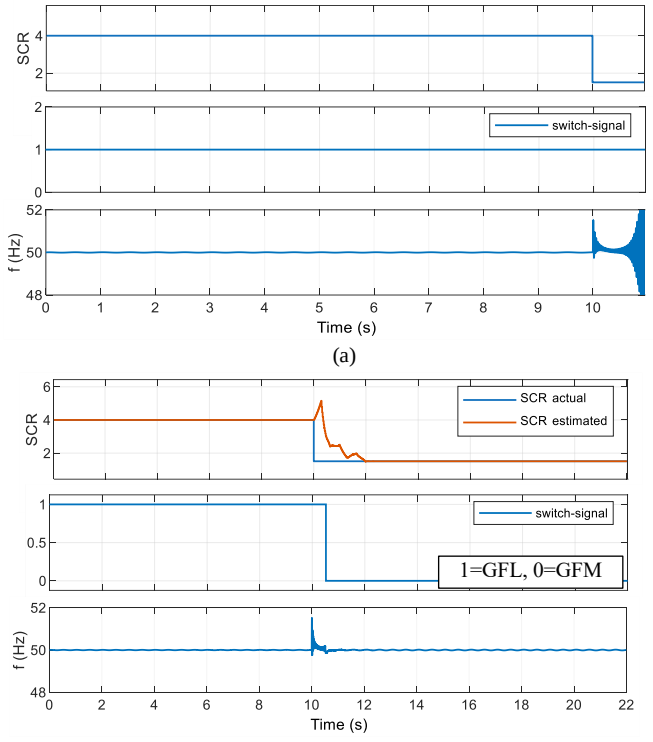

Fig. 11. System response during sudden decrease in SCR (a) without and (b) with the proposed control strategy.

As mentioned in Table 2, the detection delays (from the instant the true SCR crossed the threshold till the time it was actioned) and the root mean square error (RMSE) of the estimated SCR are satisfactory. Therefore, from the simulation studies it is evident that with the proposed control strategy the IBR switches its mode of operation automatically and effectively and maintain the operational stability of the system. The proposed method has negligible computational implications for a system that is already capable to operate in GFM mode, as the updated control scheme is implemented in the software without any hardware update. The methodology can be applicable to large systems with multiple IBRs, however, the presence of non-linearities or control dynamics can affect its performance.

TABLE 2. PERFORMANCE METRICS

Case		Detection delay	RMSE
Case 1	Gradual decrease in SCR	0.08s	2.64%
	Gradual increase in SCR	1.2s	5.05%
Case 2	Sudden increase in SCR	0.52s	11.54%
	Sudden decrease in SCR	0.72s	17%

IV. CONCLUSION

This paper presents an advanced automatic switching control strategy for IBR to switch the operational modes by using the online grid impedance estimation. The simulation studies shows that the OLS has effectively estimated the grid impedance to calculate the SCR and to generate the automatic switching signal. The proposed smooth switching control strategy produced satisfactory results to switch the IBR between GFL and GFM mode without producing the oscillations in the system response. Therefore, with the application of proposed control strategy the IBR can switch the operating mode automatically depending on the grid strength which enhances the flexibility and operational stability of the grid connected IBR.

ACKNOWLEDGMENT

This work has been conducted within UNIFORM project and supported by UKRI under Grant agreement EP/Y001575/1.

REFERENCES

[1] J. Rocabert, A. Luna et al, “Control of power converters in AC microgrids,” *IEEE Trans Power Electron*, vol. 27, no. 11, 2012.
[2] A. Singh, J. Benzaquen, and B. Mirafzal, “Current Source Generator-Converter Topology for Direct-Drive Wind Turbines,” *IEEE Trans Ind Appl*, vol. 54, no. 2, pp. 1663–1670, Mar. 2018.
[3] D. Sharma, F. Sadeque, and B. Mirafzal, “Synchronization of Inverters in Grid Forming Mode,” *IEEE Access*, vol. 10, pp. 41341–41351, 2022.
[4] X. Wang, M. G. Taul, et al, “Grid-Synchronization Stability of Converter-Based Resources - An Overview,” *IEEE Open Journal of Industry Applications*, vol. 1, pp. 115–134, 2020.
[5] H. Zhang, W. Xiang, et al, “Grid Forming Converters in Renewable Energy Sources Dominated Power Grid: Control Strategy, Stability, Application, and Challenges,” *Journal of Modern Power Systems and Clean Energy*, vol. 9, no. 6, pp. 1239–1256, Nov. 2021.
[6] F. Sadeque, D. Sharma, and B. Mirafzal, “Seamless Grid-Following to Grid-Forming Transition of Inverters Supplying a Microgrid,” in *Conference Proceedings - IEEE Applied Power Electronics Conference and Exposition - APEC*, Institute of Electrical and Electronics Engineers Inc., 2023, pp. 594–599
[7] M. Kwon, S. Park, et al, “Unified control scheme of grid-connected inverters for autonomous and smooth transfer to stand-alone mode,” *IEEE Trans Power Electron*, vol. 37, no. 1, pp. 416–425, Jan. 2022.
[8] S. Maleki, T. Chakraborty, et al, “Utility-Based Grid Forming Inverters Applications: Seamless Transition and Power Oscillation Damping,” *Proceedings of the IEEE Power Engineering Society Transmission and Distribution Conference*, vol. 2022-April, 2022.
[9] W. Wang, K. Sun, K. J. Li, Y. Dong, Z. Zhang, and Y. Sun, “Smooth switching control strategy with complete process of frequency support for photovoltaic grid-connected converter,” *International Journal of Electrical Power and Energy Systems*, vol. 151, Sep. 2023.
[10] Z. Zhang and Y. Yang, “Control Flexibility of Power Converters for Seamless Transition between Grid-Following and Grid-Forming Modes,” in *PEAS 2023 - 2023 IEEE 2nd International Power Electronics and Application Symposium, Conference Proceedings*, Institute of Electrical and Electronics Engineers Inc., 2023, pp. 1015–1020.
[11] J. Yu, W. Liu, et al, “An improved grid impedance estimator for grid-forming converters in consideration of controller dynamics,” *International Journal of Electrical Power and Energy Systems*, vol. 154, Dec. 2023.
[12] J. H. Suárez, H. M. T. C. Gomes, et al, “Grid impedance estimation for grid-tie inverters based on positive sequence estimator and morphological filter, ”*Electrical Engineering*, vol.102, no.3, Sep. 2020.
[13] B. Liu, Z. Liu, and J. Liu, “A Noninvasive Feeder Impedance Estimation Method for Parallel Inverters in Microgrid Based on Load Harmonic Current,” *IEEE Trans Power Electron*, vol. 36, no. 7, pp. 7354–7359, Jul. 2021
[14] F. Javier Toledo, J. M. Blanes, and V. Galiano, “Two-Step Linear Least-Squares Method for Photovoltaic Single-Diode Model Parameters Extraction,” *IEEE Transactions on Industrial Electronics*, vol. 65, no. 8, pp. 6301–6308, Aug. 2018.